*ANZIAM J.* 59(2017), 167–182
doi:10.1017/S1446181117000311

# SEMI-ANALYTICAL SOLUTIONS FOR THE BRUSSELATOR REACTION–DIFFUSION MODEL

H. Y. ALFIFI[1]

(Received 10 November, 2016; accepted 3 May, 2017; first published online 23 October 2017)

**Abstract**

Semi-analytical solutions are derived for the Brusselator system in one- and two-dimensional domains. The Galerkin method is processed to approximate the governing partial differential equations via a system of ordinary differential equations. Both steady-state concentrations and transient solutions are obtained. Semi-analytical results for the stability of the model are presented for the identified critical parameter value at which a Hopf bifurcation occurs. The impact of the diffusion coefficients on the system is also considered. The results show that diffusion acts to stabilize the systems better than the equivalent nondiffusive systems with the increasing critical value of the Hopf bifurcation. Comparison between the semi-analytical and numerical solutions shows an excellent agreement with the steady-state transient solutions and the parameter values at which the Hopf bifurcations occur. Examples of stable and unstable limit cycles are given, and Hopf bifurcation points are shown to confirm the results previously calculated in the Hopf bifurcation map. The usefulness and accuracy of the semi-analytical results are confirmed by comparison with the numerical solutions of partial differential equations.

2010 *Mathematics subject classification*: primary 35K57; secondary 34C05, 34K18.

*Keywords and phrases*: semi-analytical solutions, reaction–diffusion, Brusselator model, Hopf bifurcations, limit cycle, system of ordinary differential equations.

## 1. Introduction

Many chemical applications have been modelled and investigated using systems of ordinary differential equations (ODE) and partial differential equations (PDE) by both theoreticians and practical researchers for many decades. Previous work in this area has considered Belousov–Zhabotinsky (BZ) reactions [7], reversible Selkov models [4], cubic autocatalytic reactions [8, 21] and pellet systems [23] (see also the references therein). These applications have described many oscillatory phenomena in daily life using continuous-flow well-stirred tank reactors (CSTRs). CSTRs have

[1]Department of Basic Sciences, College of Education, Imam Abdulrahman Bin Faisal University, Dammam, Saudi Arabia; e-mail: hyalfifi@iau.edu.sa.

shown excellent results in experimental and theoretical studies of oscillatory chemical systems [5, 6, 21, 23].

The Brusselator is an intramolecular chemical reaction system used to drive cooperative phenomena in chemically reacting systems. It is a simple two-species (nonlinear) model of the BZ reaction, introduced by Prigogene and Lefever [26]. A standard Brusselator system can be described by a system of ODEs

$$u_t = a - (b+1)u + u^2 v, \quad v_t = bu - u^2 v, \tag{1.1}$$

where $u$ and $v$ represent the concentrations of reactants, and $a > 0$ and $b > 0$ are control parameters. Many methods have been used extensively in the literature for the steady-state solution and stability analysis of (1.1). Brown and Davidson [11] considered global steady-state bifurcations, Peng and Wang [25] assessed the existence of nonconstant positive steady-state solutions, Li and Wang [18] evaluated the existence and stability of Hopf bifurcation periodic solutions, You [32] considered the global dynamics and Biazar and Ayati [10] proposed a numerical solution for the Brusselator system by applying the Adomian decomposition method [2].

The effects of diffusion on the Brusselator reaction have also been explored extensively. Recently, Ma and Hu [20] considered the structure of nonnegative steady-state solutions for a Brusselator model with a one-dimensional (1-D) geometry. The theory of global bifurcation was applied and the concentration of reactant was treated as a bifurcation parameter. An explicit formula for nonconstant steady states was derived for the system. The researchers also illustrated some examples to confirm their analytical results. Further, Guo et al. [14] derived the diffusive Brusselator system under homogeneous Neumann boundary conditions. Hopf bifurcation was shown for both the ODE and PDE models. The bifurcation direction and stability of periodic solutions were found using centre manifold theory. Comparisons were made between numerical simulations and the analytical results to confirm the solutions. In another study, Xu et al. [31] showed a semi-discrete reaction–diffusion of the Brusselator system. Here, an analysis of Turing instability theory was applied. Numerical simulations of the model were performed in the Turing instability region and various patterns were identified. The impacts of the system parameters and diffusion coefficients on the patterns were also visually shown.

The numerical solutions of reaction–diffusion Brusselator systems have been investigated extensively by many authors. Recently, Jiwari and Yuan [16] considered a modified cubic B-spline differential quadrature method, Twizell et al. [28] derived a second-order finite-difference method and Adomian [3] and Wazwaz [30] obtained numerical results using the decomposition method. Also, Ang [9] assessed the dual-reciprocity boundary element method, Mittal and Jiwari [24] considered a numerical study using the differential quadrature method, Khan et al. [17] studied a reaction–diffusion Brusselator system using the homotopy perturbation method and Hundsdorfer et al. [29] applied the Runge–Kutta–Chebyshev method [1].

A semi-analytical method for solving reaction–diffusion systems has been developed for various other problems, such as pellet systems [23], logistic equations [5], BZ reactions [7], feedback control for microwave heating [19], Nicholson's

https://doi.org/10.1017/S1446181117000311 Published online by Cambridge University Press

blowflies equation [6], the steady-state microwave heating of finite 1-D and two-dimensional (2-D) slabs [22], the reversible Selkov model with feedback delay [4] and mixed quadratic–cubic autocatalytic reactions [8]. In 2002, Marchant [21] developed the Gray and Scott cubic autocatalytic system in a 1-D domain. They derived an ODE system using the Galerkin method as an approximation to the PDE model, and applied bifurcation theory to find the semi-analytical steady-state solutions and bifurcation maps. Further, Alfifi et al. [5] presented semi-analytical solutions for a class of generalized logistic equations. They considered point and distributed delays for both 1-D and 2-D domains. A system of ODEs with delay was obtained using the Galerkin method, and semi-analytical solutions for the stability analysis of the system were found. Excellent comparisons were made between the semi-analytical results and numerical solutions of the governing PDEs for all the application problems that were solved using the semi-analytical method.

In this paper, the Brusselator system in 1-D and 2-D reaction–diffusion cells is discussed. Nevertheless, the paper also presents various aims of the Brusselator model, such as providing illustrations on how the Galerkin averaging method is crucial in the calculation of the model to ascertain how diffusion can affect the model, and provide explanations of how calculations can be derived to predict the Hopf bifurcations for the Brusselator model. Note that we mainly consider the parameter $b$ as a Hopf bifurcation parameter in the system.

This paper is organized as follows. The application of the Galerkin technique to solve ODE systems is explored in Section 2, and both the steady-state solutions pertaining to ODE systems (semi-analytical solutions) and solutions of numerically administered PDEs are determined in Section 3. Section 4 presents a stability analysis to determine the Hopf bifurcation points, and there is a comparison of the numerical and semi-analytical models explored in this paper. A brief conclusion is presented in Section 5.

## 2. The semi-analytical model

**2.1. Governing equations** The diffusive Brusselator for a 2-D geometry is a nonlinear system of PDEs, which is expressed as follows:

$$\begin{aligned} u_t &= \alpha(u_{xx} + u_{yy}) + a - (b+1)u + u^2v, \\ v_t &= \alpha(v_{xx} + v_{yy}) + bu - u^2v, \\ u_x &= v_x = 0 \quad \text{at } x = 0, \\ u_y &= v_y = 0 \quad \text{at } y = 0, \\ u &= v = 0 \quad \text{at } x, y = 1 \text{ and } t = 0. \end{aligned} \tag{2.1}$$

Here, $u = u(x, y, t)$ and $v = v(x, y, t)$ represent dimensionless concentrations of two reactants at time $t$. The 1-D model can be obtained by simplification of the system (2.1), where there is no $y$-variation, that is, $y = 0$. It should be noted that the terms $u$ and $v$ are the activator and inhibitor, respectively; they substantiate the depletion, resulting

https://doi.org/10.1017/S1446181117000311 Published online by Cambridge University Press

in effective inhibition. This is an open system. The reactor has a permeable boundary at $x, y = \pm 1$, joined to a reservoir that contains $u$ and $v$ at constant concentrations. At the centre of the domain where $x, y = 0$, there is a zero-flux boundary condition. Hence, the solution is symmetrical around the centre of the concentrations $x, y = 0$. The system has three parameters: $\alpha$ is the diffusion coefficient of the two reactants, while $a > 0$ and $b > 0$ are control parameters during the reaction process. In addition, we consider $u_a$ and $v_a$ to be the positive initial concentrations in the system. Note that the system has a unique steady-state solution [14, 18, 28], and we let $(u_s, v_s)$ represent steady-state concentrations at the centre of the domain $x, y = 0$.

A Crank–Nicholson finite-difference scheme [5] and a Runge–Kutta fourth-order technique [23] are presented for the numerical solutions of PDEs and ODEs, respectively. The spatial and temporal discretizations utilized in all figures and examples are $\Delta x = 0.05$ and $\Delta t = 5 \times 10^{-3}$. The percentage error (the percentage error is the absolute value of the difference divided by the correct value times 100) is used to calculate the difference between the numerical and the two-term semi-analytical solutions.

**2.2. The Galerkin method** The semi-analytical system for (2.1) has been found using the Galerkin method [13] in the 1-D and 2-D domains. In this method, there is the consideration of a spatial form of the profile concentration [5, 21, 23]. The Galerkin method is an analytical technique that uses orthogonality of a set of basis functions to replace PDEs with an ODE model. This method has been used to solve problems in structure mechanics, dynamics, fluid flow, neutron transport and so on [13]. In the 1-D model, we use the following trial function expansion:

$$\begin{aligned} u(x,t) &= u_1(t)\cos\left(\frac{\pi x}{2}\right) + u_2(t)\cos\left(\frac{3\pi x}{2}\right), \\ v(x,t) &= v_1(t)\cos\left(\frac{\pi x}{2}\right) + v_2(t)\cos\left(\frac{3\pi x}{2}\right), \end{aligned} \tag{2.2}$$

which represents a two-term method. Expansion (2.2) satisfies the boundary conditions described in (2.1) (for further details, see [5, 6, 21]). Thus, the free parameters in this expansion are created from evaluating averaged versions of the governing equation, weighted by the basis functions $\cos(\pi x/2)$ and $\cos(3\pi x/2)$. Thereafter, there is a system of the following four ODEs:

$$\begin{aligned} \frac{du_1}{dt} &= -\frac{\pi^2}{4}\alpha u_1 + \frac{1}{2}u_2^2 v_1 + \frac{1}{4}u_1^2 v_2 + \frac{1}{2}u_1 u_2 v_1 + \frac{3}{4}u_1^2 v_1 + \frac{4}{\pi}a + u_1 u_2 v_2 - b u_1 - u_1, \\ \frac{dv_1}{dt} &= -\frac{\pi^2}{4}\alpha v_1 - \frac{1}{4}u_1^2 v_2 - \frac{1}{2}u_2^2 v_1 - \frac{3}{4}u_1^2 v_1 - \frac{1}{2}u_1 u_2 v_1 - u_1 u_2 v_2 + b u_1, \\ \frac{du_2}{dt} &= -\frac{9\pi^2}{4}\alpha u_2 + \frac{1}{2}u_1^2 v_2 + \frac{3}{4}u_2^2 v_2 + \frac{1}{4}u_1^2 v_1 - \frac{4}{3\pi}a + u_1 u_2 v_1 - b u_2 - u_2, \\ \frac{dv_2}{dt} &= -\frac{9\pi^2}{4}\alpha v_2 - \frac{1}{2}u_1^2 v_2 - \frac{3}{4}u_2^2 v_2 - \frac{1}{4}u_1^2 v_1 - u_1 u_2 v_1 + b u_2. \end{aligned} \tag{2.3}$$

https://doi.org/10.1017/S1446181117000311 Published online by Cambridge University Press

The series in (2.2) has been truncated after two terms. The number of terms that are used in the truncated series is used to illustrate a trade-off between the accuracy and complexity of the ODE system for the semi-analytical solution. It is found that a two-term method produces superior accuracy without excessive expression swell. Evidently, it is revealed that sufficient accuracy with little expression swell is provided by the two-term method. As (2.2) includes two different trial function terms, system (2.3) is composed of four different ODEs. Moreover, the one-term solutions are created by setting $u_2 = v_2 = 0$.

For the 2-D spatial domain, we use the following expansion:

$$\begin{aligned} u(x,y,t) &= u_1(t)\cos\left(\frac{\pi x}{2}\right)\cos\left(\frac{\pi y}{2}\right) + u_2(t)\cos\left(\frac{3\pi x}{2}\right)\cos\left(\frac{\pi y}{2}\right) \\ &\quad + u_2(t)\cos\left(\frac{\pi x}{2}\right)\cos\left(\frac{3\pi y}{2}\right) + u_3(t)\cos\left(\frac{3\pi x}{2}\right)\cos\left(\frac{3\pi y}{2}\right), \\ v(x,y,t) &= v_1(t)\cos\left(\frac{\pi x}{2}\right)\cos\left(\frac{\pi y}{2}\right) + v_2(t)\cos\left(\frac{3\pi x}{2}\right)\cos\left(\frac{\pi y}{2}\right) \\ &\quad + v_2(t)\cos\left(\frac{\pi x}{2}\right)\cos\left(\frac{3\pi y}{2}\right) + v_3(t)\cos\left(\frac{3\pi x}{2}\right)\cos\left(\frac{3\pi y}{2}\right). \end{aligned} \tag{2.4}$$

The trial function expansion (2.4) also satisfies the boundary conditions at $x, y = \pm 1$, which are explained in (2.1). Note that each expansion in (2.4) has four terms, but, by symmetry, two of the terms have the same coefficient. The free parameters in the 2-D case are shown by evaluating the averaged versions of the governing PDEs, weighted by the basis functions $\cos(\pi x/2)\cos(\pi y/2)$, $\cos(3\pi x/2)\cos(\pi y/2)$ and $\cos(3\pi x/2)\cos(3\pi y/2)$. Then we have the following system of six ODEs:

$$\begin{aligned} \frac{du_1}{dt} &= -\frac{\pi^2}{2}\alpha u_1 + \frac{1}{2}u_2^2 v_3 - b u_1 + \frac{1}{4}u_3^2 v_1 + \frac{7}{8}u_1^2 v_1 + \frac{3}{8}u_1^2 v_2 + \frac{7}{4}u_1 u_2 v_2 \\ &\quad + \frac{1}{16}u_1^2 v_3 - u_1 + \frac{3}{4}u_2^2 v_2 + \frac{1}{2}u_1 u_2 v_3 + \frac{1}{2}u_1 u_3 v_3 + \frac{9}{16}u_1^2 v_1 + u_2 u_3 v_2 \\ &\quad + \frac{3}{4}u_1 u_2 v_1 + \frac{1}{2}u_2 u_3 v_1 + \frac{1}{8}u_1 u_3 v_1 + \frac{16}{\pi^2}a, \\ \frac{dv_1}{dt} &= -\frac{\pi^2}{2}\alpha v_1 - \frac{9}{16}u_1^2 v_1 - \frac{1}{2}u_2 u_3 v_1 - \frac{1}{2}u_1 v_3 u_3 - \frac{1}{16}u_1^2 v_3 - u_2 u_3 v_2 \\ &\quad + b u_1 - \frac{1}{4}u_3^2 v_1 - \frac{3}{8}u_1^2 v_2 - \frac{1}{2}u_2^2 v_3 - \frac{7}{4}u_1 u_2 v_2 - \frac{3}{4}u_2^2 v_2 - \frac{1}{2}u_1 u_3 v_2 \\ &\quad - \frac{3}{4}u_1 v_1 u_2 - \frac{1}{2}u_1 u_2 v_3 - \frac{7}{8}u_2^2 v_1 - \frac{1}{8}u_1 u_3 v_1, \\ \frac{du_2}{dt} &= -\frac{5\pi^2}{2}\alpha u_2 - \frac{3}{16}u_2^2 v_3 + \frac{3}{8}u_2^2 v_1 + \frac{7}{16}u_1^2 v_2 + \frac{3}{4}u_1 u_2 v_2 + \frac{1}{2}u_1 v u_2 v_3 \\ &\quad + \frac{21}{16}u_2^2 v_2 + \frac{1}{2}u_2 u_3 v_1 - \frac{16}{3\pi^2}a + \frac{3}{8}u_3^2 v_2 - u_2 + \frac{3}{4}u_2 u_3 v_3 + \frac{3}{16}u_1^2 v_1 \\ &\quad + \frac{1}{8}u_1^2 v_3 + \frac{1}{2}u_1 u_3 v_2 + \frac{7}{8}u_1 u_2 v_1 + \frac{1}{4}u_1 u_3 v_1 + \frac{3}{8}u_2 u_3 v_2 - b u_2, \end{aligned} \tag{2.5}$$

https://doi.org/10.1017/S1446181117000311 Published online by Cambridge University Press

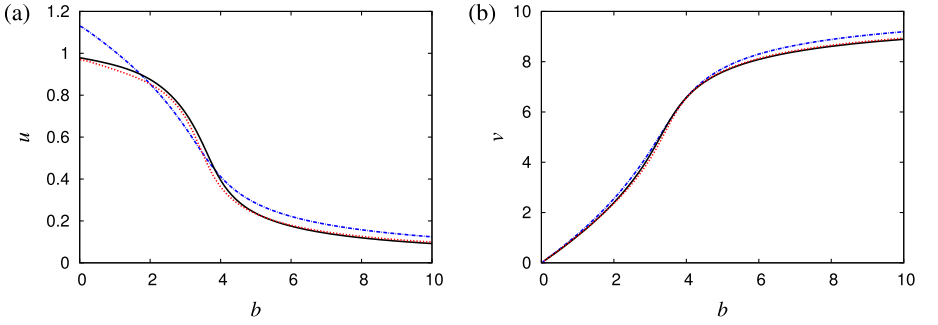


FIGURE 1. The steady-state reactant concentrations $u$ and $v$ against $b$ at $x = 0$, for the 1-D spatial domain. The blue dashed line and black solid line represent, respectively, one-term and two-term semi-analytical solutions, and the red dotted line represents the specification used for the PDEs of (2.1). The parameters are $a = 1$, $u_a = v_a = 1$ and $\alpha = 0.05$ (colour available online).

$$\begin{aligned}
\frac{dv_2}{dt} =& -\frac{5\pi^2}{2}\alpha v_2 - \frac{3}{16}u_1^2 v_1 - \frac{3}{8}u_3^2 v_2 - \frac{7}{16}u_1^2 v_2 - \frac{3}{8}u_2 u_3 v_2 - \frac{7}{8}u_1 u_2 v_1 \\
& - \frac{3}{16}u_2^2 v_3 - \frac{3}{4}u_2 v_3 u_3 - \frac{1}{2}u_1 v_3 u_2 - \frac{1}{4}u_1 v_1 u_3 - \frac{1}{2}u_2 v_1 u_3 - \frac{3}{8}u_2^2 v_1 \\
& - \frac{21}{16}u_2^2 v_2 - \frac{1}{8}u_1^2 v_3 + b u_2 - \frac{1}{2}u_1 v_2 u_3 - \frac{3}{4}u_1 u_2 v_2, \\
\frac{du_3}{dt} =& -\frac{9\pi^2}{2}\alpha u_3 + \frac{3}{4}u_2^2 v_3 + \frac{1}{16}u_1^2 v_1 + \frac{3}{8}u_2^2 v_2 + \frac{1}{4}u_1^2 v_3 + \frac{9}{16}u_3^2 v_3 - u_3 + \frac{1}{4}u_1^2 v_2 \\
& + u_1 u_2 v_2 + \frac{1}{2}u_1 u_2 v_1 - b u_3 + \frac{1}{2}u_1 v_1 u_3 + \frac{16}{9\pi^2}a + \frac{3}{2}u_2 u_3 v_2 + \frac{1}{2}u_2^2 v_1 \\
\frac{dv_3}{dt} =& -\frac{9\pi^2}{2}\alpha v_3 + \frac{1}{16}u_1^2 v_1 - \frac{3}{8}u_2^2 v_2 - \frac{3}{4}u_2^2 v_3 - u_1 u_2 v_2 + b u_3 + \frac{9}{16}u_3^2 v_3 \\
& - \frac{1}{2}u_1 u_3 v_1 - \frac{1}{2}u_2^2 v_1 - \frac{1}{4}u_1^2 v_3 - \frac{3}{2}u_2 u_3 v_2 - \frac{1}{2}u_1 u_2 v_1 - \frac{1}{4}u_1^2 v_2.
\end{aligned}$$

## 3. Steady-state solutions

Figure 1 shows the steady-state reactant concentrations $u$ and $v$ against $b$ for the 1-D spatial domain. It illustrates both the two- and one-term semi-analytical models as well as numerical solutions obtained at the domain centre, $x = 0$. The parameters are $\alpha = 0.05$, $u_a = v_a = 1$ and $a = 1$. There is a unique pattern in the steady-state solutions for the reactant concentrations. Figure 1(a) shows that $u$ decreases as $b$ increases, before approaching a minimum at a large value of $b$. However, the curve in Figure 1(b) for $v$ increases as $b$ increases. Hence, for a large value of $b$, $u$ is near zero, while $v$ increases linearly. There is an excellent comparison existing between the numerical and the two-term semi-analytical solutions, with not more than 1.5% error for all the $b$ values over the chosen domain of up to $b = 10$. This behaviour is qualitatively similar to the nondiffusive case with $\alpha = 0$.

https://doi.org/10.1017/S1446181117000311 Published online by Cambridge University Press

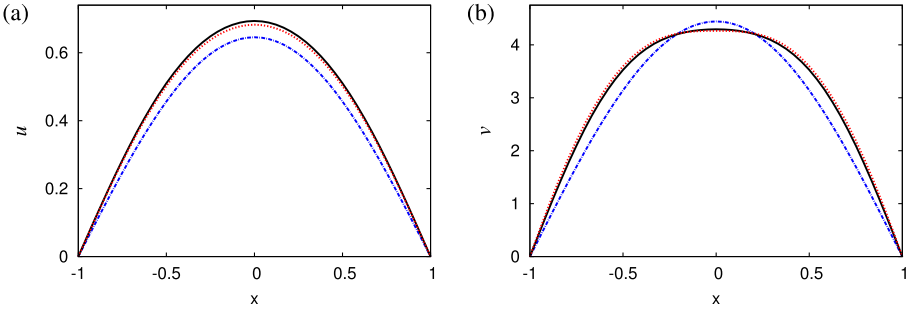


FIGURE 2. The steady-state reactant concentrations $u$ and $v$ against $x$, for the 1-D spatial domain. Shown are the one-term (blue dashed line) and two-term (black solid line) semi-analytical solutions and numerical solutions (red dotted line) of the governing PDEs. The parameters are $a = 1$, $b = 3$, $u_a = v_a = 1$ and $\alpha = 0.05$ (colour available online).

Figure 2 shows the steady-state profiles $u$ and $v$ against $x$, for the 1-D spatial domain. It illustrates the one-term and two-term semi-analytical and numerical solutions of the governing PDEs; the parameters are $a = 1$, $b = 3$, $u_a = v_a = 1$ and $\alpha = 0.05$. The solutions for the reactant concentrations $u$ and $v$ have a single hump; all solutions are shown. In Figure 2(a), the one-term peak solution is $u = 0.65$ at $x = 0$. The two-term solution has a density of $u = 0.69$ at $x = 0$, which is closer to the numerical density of $u = 0.70$. For Figure 2(b), the numerical solution at $x = 0$ is $v = 4.27$, while the one- and two-term solutions at $x = 0$ are $v = 4.44$ and 4.29, respectively. Observe that the comparisons between the two-term semi-analytical solutions and numerical solutions of the governing PDEs are excellent over the whole domain, with an error of less than 2%. The one-term approximation is reasonably accurate at the centre of the domain $x = 0$, with no greater than 7% error with the numerical solution. Therefore, the two-term solution is an outstanding model, as it better approximates the solution profiles in all domain regions.

Figure 3 shows steady-state reactant concentrations $u$ and $v$ against $b$, for the 2-D spatial domain. They illustrate the numerical and the semi-analytical (one- and two-term) solutions at the domain centre $x, y = 0$. The parameters are $\alpha = 0.05$, $u_a = v_a = 1$ and $a = 1$. The behaviour in this figure is qualitatively identical to the 1-D case. Hence, at a large value of $b$, $v$ increases linearly, while $u$ approaches zero. Again, there is a good comparison with less than 7% error between the numerical and the two-term model solutions for all values of $b$ over the domain that are chosen up to $b = 10$.

Figure 4(a) and (b) show the steady-state concentration profiles $u$ and $v$ against $x$, for the 2-D spatial domain. It illustrates the numerical solution of the governing PDEs (2.1) and the semi-analytical one for the one-term and two-term solutions of (2.3). The parameters used are $a = b = 3$, $u_a = v_a = 1$ and $\alpha = 0.2$. The figure also shows the profile solutions at the domain centre at $y = 0$. A single hump is shown for each solution of the concentrations $u$ and $v$. At the centre of the domain $x = 0$, the two-term model and numerical solutions have densities of $(u, v) = (1.81, 1.07)$

https://doi.org/10.1017/S1446181117000311 Published online by Cambridge University Press

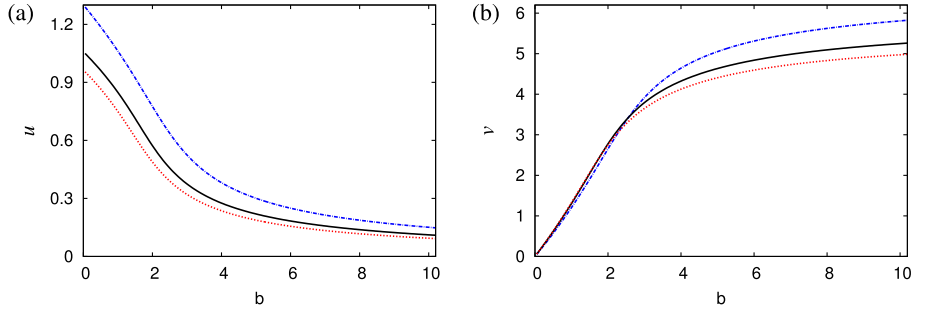


FIGURE 3. The steady-state reactant concentrations $u$ and $v$ against $b$, for the 2-D spatial domain. The blue dashed line and black solid line represent one-term and two-term solutions of the semi-analytical model and the red dotted line represents the specification used for the PDEs of (2.1). The parameters are $\alpha = 0.05$, $u_a = v_a = 1$ and $a = 1$ (colour available online).

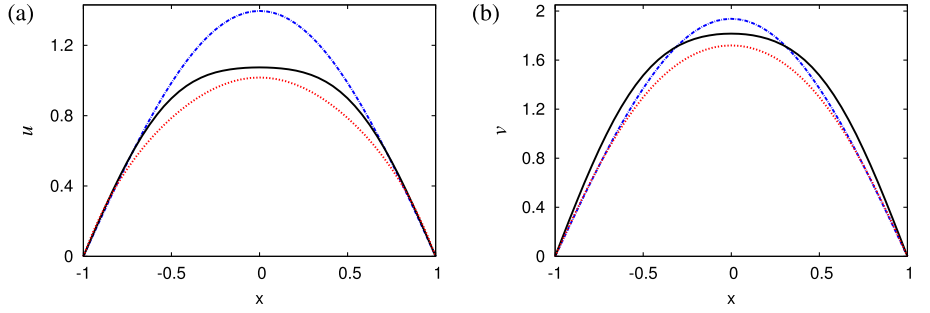


FIGURE 4. The steady-state reactant concentrations $u$ and $v$ against $x$, for the 2-D spatial domain. The one-term (blue dashed line) and two-term (black solid line) semi-analytical solutions and numerical solutions (red dotted line) of the governing PDEs of (2.1) are shown. The parameters are $a = b = 3$, $u_a = v_a = 1$ and $\alpha = 0.2$ (colour available online).

and $(u, v) = (1.72, 1.02)$, respectively. Observe that the two-term model compares well with the numerical solution. They show less than 5% errors, while the one-term approximations are quite large at the centre of the domain. Hence, the two-term model gives a better approximation of the solution profiles throughout the domain.

Note that at extremely small values of the diffusion coefficient $\alpha$, the steady-state solutions of the governing PDE model (2.1) and ODE systems (2.3) and (2.5) are converged to an equilibrium point $\approx(a, b/a)$ when $1 - b + a^2 > 0$. This result is quite similar to that obtained previously by many authors; for more details, see [16, 17, 28, 30].

## 4. Stability analysis and Hopf bifurcations

**4.1. Theoretical framework** In this section, we explain the method used to assess the stability and Hopf bifurcation points of the semi-analytical systems (2.3) and (2.5).

https://doi.org/10.1017/S1446181117000311 Published online by Cambridge University Press

A Hopf bifurcation denotes the appearance of periodic solutions in the neighbourhood of a steady state whose stability changes due to the crossing of a conjugate pair of eigenvalues over the imaginary axis [27]. The theory of Hopf bifurcations for ODE systems is described in texts on bifurcation theory and dynamical systems; for further details, see [12, 15].

For the 1-D geometry, Hopf points are found by expanding in a Taylor series around the steady-state solution, as follows:

$$u_i = u_{is} + \epsilon c_i e^{-\mu t}, \quad v_i = v_{is} + \epsilon g_i e^{-\mu t} \quad \text{where } i = 1, 2,\ \epsilon \ll 1. \tag{4.1}$$

Then the system (4.1) is substituted into an ODE system as illustrated in equation (2.3) as well as linearized around the steady state. Notably, the Jacobian matrix of eigenvalues explores the development of a small system perturbation, which shows the characteristic equation of the growth rate $\mu$. We set $\mu = iw$ in the characteristic equation and separate the real and imaginary parts, which are termed $R$ and $I$, respectively. Here, the Hopf bifurcation points for the 1-D model are obtained by solving the system of equations

$$R = I = \frac{du_1}{dt} = \frac{dv_1}{dt} = \frac{du_2}{dt} = \frac{dv_2}{dt} = 0,$$

where $du_i/dt$ and $dv_i/dt$ are the steady-state systems of (2.3).

The technique for solving Hopf bifurcation points in the 2-D case is similar to the 1-D case. Therefore, the curve of Hopf bifurcation points can be obtained by solving the conditions

$$R = I = \frac{du_1}{dt} = \frac{dv_1}{dt} = \frac{du_2}{dt} = \frac{dv_2}{dt} = \frac{du_3}{dt} = \frac{dv_3}{dt} = 0.$$

**4.2. Hopf bifurcation regions and limit cycles** A semi-analytical map in which Hopf bifurcations occur is obtained and compared with numerical results in this section. The effects of the diffusion coefficient on the system are also shown with some numerical examples related to limit cycles.

In this case, the figure has the black solid line representing the two-term semi-analytical solution and the red crosses representing the numerical solution of the PDEs.

Figure 5 shows the Hopf bifurcation curves in the $a$–$b$ diagram, for the 1-D (Figure 5(a)) and 2-D domains (Figure 5(b)). The two-term semi-analytical and numerical solutions are shown. The parameters used are $\alpha = 0.05$ and $u_a = v_a = 1$. The stability curve for the two-term semi-analytical ODE systems and numerical solutions divides the parameter space into two regions: the first is a stable region (upper region), while, in the other, they are all unstable (lower region). Figures 5(a) and 5(b) show that as the parameter $a$ increases, the critical value of $b$, at which Hopf bifurcations first occur, also increases. Evidently, it can be noted that the two predictions pertaining to the two-term semi-analytical solutions agree with the numerical computations with an error not exceeding 5% for all $b$ choices.

We also consider some comparisons for the special case, when the parameters are $a = 5$ and $\alpha = 0.05$ for the 1-D case. Here, the Hopf bifurcation points obtained

https://doi.org/10.1017/S1446181117000311 Published online by Cambridge University Press

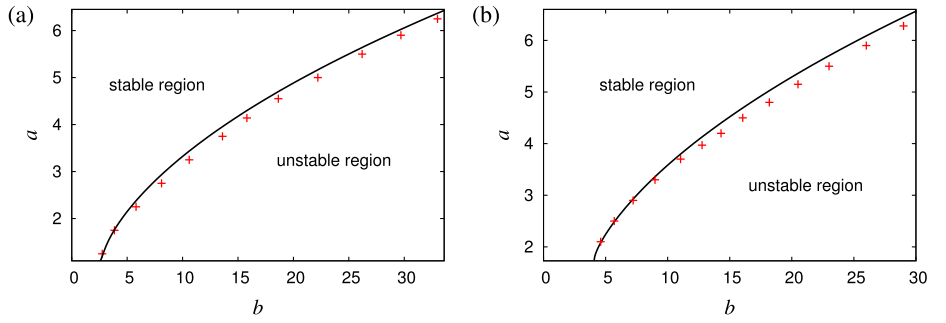


FIGURE 5. Hopf bifurcation maps in the $a$–$b$ map. The upper figure is the 1-D geometry and the lower figure the 2-D geometry. The figure has the black solid line representing the two-term semi-analytical solution and the red crosses representing the numerical solution of the PDEs (2.1). The parameters are $\alpha = 0.05$ and $u_a = v_a = 1$ (colour available online).

were $b_c \simeq 21.7, 17.5$ and 20.9 for the numerical, one- and two-term semi-analytical solutions, respectively. The predictions of the two-term semi-analytical theory are very close to the numerical predictions, with only a difference of 3.7%. In the 2-D case, the parameters used are $a = 5.5$ and $\alpha = 0.05$. Here, the Hopf bifurcation points found were $b_c \simeq 21.6, 20.5$ and 23 for the numerical solution, one- and two-term semi-analytical solutions, respectively. There is a 5% difference between the two-term semi-analytical and numerical solutions. Hence, the semi-analytical solution is an excellent predictor of the occurrence of Hopf bifurcations.

Figure 6(a) and (b) show Hopf bifurcation curves in the $a$–$b$ map for different values of the diffusion coefficients, for the 1-D and 2-D domains. Two-term semi-analytical solutions are obtained for six different values of diffusion, namely, 0, 0.01, 0.02, 0.03, 0.04 and 0.05. We observe that appropriately chosen values of the diffusion parameter $\alpha$ can stabilize or destabilize regions of parameter space. Note that, for any fixed value of $a$ (given $b$), the system is destabilized as $\alpha$ increases, when the critical value of $b$ is decreased. However, for all different cases in Figure 6, as $a$ increases, the critical value of the proliferation rate $b$ is increased.

Figure 7(a) and (b) show Hopf bifurcation curves for the parameter $b$ versus the diffusion coefficient $\alpha$. The top figure is the 1-D case and the bottom figure the 2-D domain. The parameters are $a = 5$ for (a) and $a = 4$ for (b). The two-term semi-analytical solution is shown. In both cases, as the Hopf bifurcation parameter $b$ is increased, the diffusion coefficient $\alpha$ decreases. This figure confirms the result obtained in Figure 6. Hence, it may be concluded that the diffusion parameter $\alpha$ can affect and represent a stabilized or a destabilized system.

Figure 8(a) and (b) show the reactant concentrations $u$ and $v$ at $x = 0$ against time represented by $t$, for the 1-D spatial domain. The parameters are: $u_a = v_a = 1$, $\alpha = 0.05$ and $b = 5$, with $a = 2.3$ (upper region of Figure 5(a)). The one-term and two-term semi-analytical solutions and numerical solutions of (2.1) are obtained. The solution evolves to a steady state, with $u(0, t) \simeq 2.34$ and $v(0, t) \simeq 2.11$ as the time increases,

https://doi.org/10.1017/S1446181117000311 Published online by Cambridge University Press

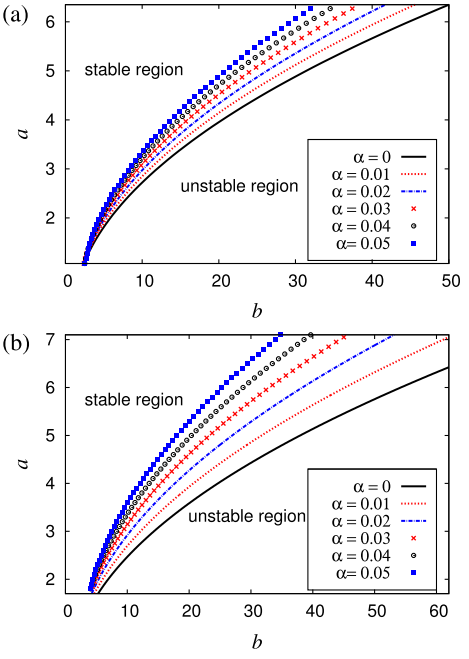


FIGURE 6. Hopf bifurcation curves in the $a$–$b$ map, for different values of $\alpha$, such as: $\alpha = 0$, 0.01, 0.02, 0.03, 0.04 and 0.05. Figures (a) and (b) are for the 1-D domain and 2-D domain, respectively. The two-term semi-analytical solutions of system (2.3) are shown (colour available online).

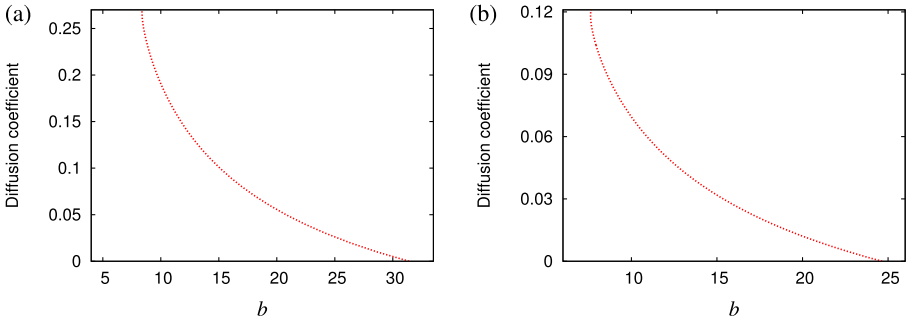


FIGURE 7. This shows the Hopf bifurcation curve in the $b$–$\alpha$ map for (a) 1-D and (b) 2-D geometries. The two-term semi-analytical solution of (2.3) is shown with $a = 5$ for (a) and $a = 4$ for (b) (colour available online).

after some initial relaxation oscillations. The comparison between the two-term semi-analytical and numerical solutions is excellent; a maximum error of only 1.6% in the steady state is observed. The difference between the numerical solution and the one-term semi-analytical solution is reasonably accurate for the concentration $u$, while the concentration $v$ is slightly higher, that is, being 15% at $b = 26$.

https://doi.org/10.1017/S1446181117000311 Published online by Cambridge University Press

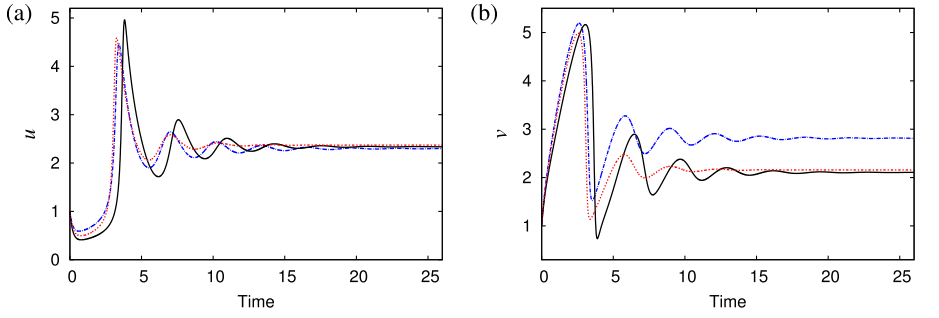


FIGURE 8. The reactant concentrations $u$ and $v$ at $x = 0$ against $t$ for the 1-D spatial domain are shown. The one- and two-term semi-analytical solutions are represented by blue dashed line and black solid line, respectively. The red dotted lines represent numerical solutions. The parameters are $a = 2.3$, $b = 5$ and $\alpha = 0.05$ (colour available online).

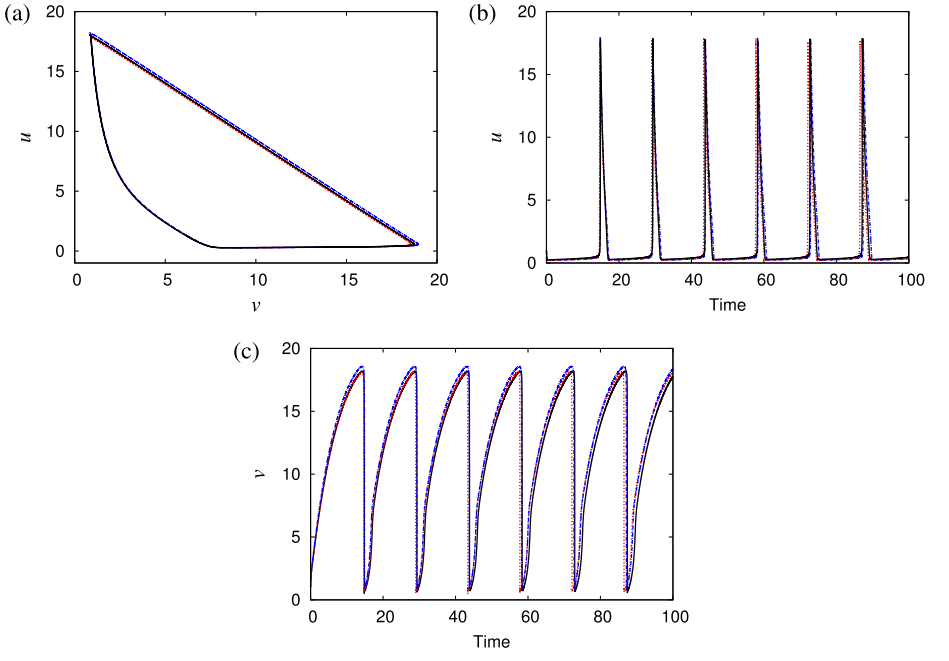


FIGURE 9. The limit cycle curve $u$ versus $v$ is shown in (a), while the reactant concentrations $u$ and $v$ at $x = 0$ against $t$, for the 1-D spatial domain, are shown in (b) and (c). The one-term (blue dashed line), two-term (black solid line) semi-analytical and numerical (red dotted line) solutions of the governing PDEs of (2.1) are represented. The parameters are $a = 2.5$, $b = 13$ and $\alpha = 0.05$.

Figure 9(a) shows a limit cycle curve of $u$ versus $v$, while Figure 9(b) and (c) show the time evolution of the reactant concentrations $u$ and $v$ versus time $t$, respectively, for the 1-D spatial domain. The parameters are: $u_a = v_a = 1$, $\alpha = 0.05$ and $b = 13$, with

https://doi.org/10.1017/S1446181117000311 Published online by Cambridge University Press

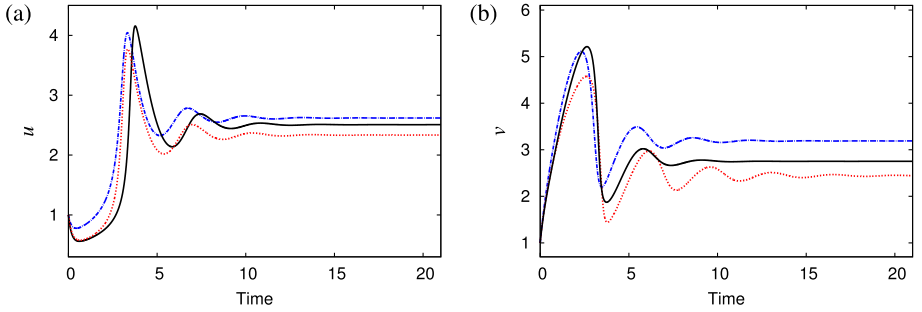


FIGURE 10. The reactant concentrations $u$ and $v$ at $x = y = 0$ against $t$ for the 2-D spatial domain are represented in (a) and (b). The one-term (blue dashed line), two-term (black solid line) semi-analytical and numerical (red dotted line) solutions of the governing PDEs of (2.1) are shown. The parameters are $a = 2.5$, $b = 5$ and $\alpha = 0.05$ (colour available online).

$a = 2.5$ (lower region of Figure 5(a)). The one- and two-term semi-analytical solutions and the numerical solutions of (2.1) are shown. The numerical period of the limit cycle of the reactant is 14.4, while the amplitudes of the limit cycle are 17.7 and 18.2 for the concentrations $u$ and $v$, respectively. The two-term semi-analytical period and amplitude are very close to the numerical results; the period is 14.5 and the amplitudes are 17.8 and 18.4 for the concentrations $u$ and $v$, respectively. The errors in the two-term semi-analytical values are less than 1%. In addition, the one-term semi-analytical solution is reasonable compared to the numerical solution.

Figure 10(a) and (b) show the reactant concentrations $u$ and $v$ against time $t$ ($x = y = 0$), for the 2-D spatial domain. The parameters are: $u_a = v_a = 1$, $\alpha = 0.05$, $b = 5$ and $a = 2.5$; note that this point is chosen from the upper region of Figure 5(b). The one-term and two-term semi-analytical solutions and numerical solutions of (2.1) are drawn. The solution evolves to a steady state with $u(0, 0, t) \simeq 2.51$ and $v(0, 0, t) \simeq 2.73$, as the time increases after some initial relaxation oscillations. The errors between the numerical solutions and the two-term semi-analytical solutions are less than 7% at the steady state for reactant concentrations $u$ and $v$, respectively. Here, observe that the two-term semi-analytical solution gives a good approximation compared to the governing PDE solution. The one-term semi-analytical solution is reasonably accurate for the concentration $u$, while $v$ is slightly higher in the steady state.

Figure 11(a) and (b) show the time evolution of the reactant concentrations $u$ and $v$ against time $t$, for the 2-D spatial domain. Moreover, Figure 11(c) shows a limit cycle curve of $u$ versus $v$. The parameters are: $u_a = v_a = 1$, $\alpha = 0.05$ and $b = 11$, with $a = 2.5$ (from the lower region of Figure 5(b)). Here, a limit cycle occurs for this choice of parameters. The one- and two-term semi-analytical solutions and the numerical solutions of (2.1) are shown. The numerical period of the limit cycle of the reactant is 9.8, while the amplitudes of the limit cycle are 9.9 and 11.1 for the reactant concentrations $u$ and $v$, respectively. The two-term semi-analytical period is 8.4, while the amplitudes are 10.9 and 12.3 for the concentrations $u$ and $v$, respectively. The errors

https://doi.org/10.1017/S1446181117000311 Published online by Cambridge University Press

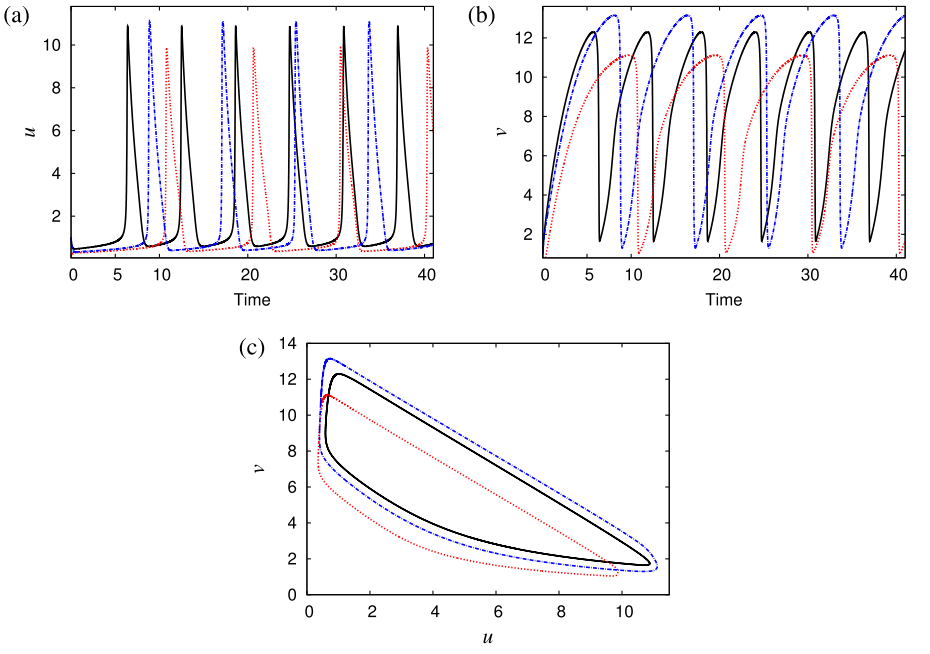


FIGURE 11. The limit cycle curve $u$ versus $v$ is shown in (a), while the reactant concentrations $u$ and $v$ at $x = y = 0$ against $t$ for the 2-D spatial domain are shown in (b) and (c). The one-term semi-analytical solutions are represented by blue dashed line while black solid line represents the two-term semi-analytical solutions. The red dotted lines represent numerical solutions. The parameters are $a = 2.5$, $b = 11$ and $\alpha = 0.05$ (colour available online).

for the 2-D domain are slightly larger than those for the 1-D domain, but these are less than 15%.

## 5. Conclusions

A lower-order semi-analytical model for the Brusselator system in one- and two-dimensional domains is given in this paper. The Galerkin method is used to produce an ODE system. We successfully found steady-state solutions for the system, constructed a Hopf bifurcation diagram and performed a stability analysis of the Hopf bifurcation points. A Hopf bifurcation map is obtained and the effects of diffusion coefficients in the system are studied. We observe that increasing the diffusion coefficients within the system can have a stabilizing effect, and we provide an example of stable and unstable limit cycles. We also demonstrate that a two-term system provides greater accuracy than a one-term system. Comparisons of the two-term semi-analytical and the PDE systems (numerical solutions) further show the utility of the semi-analytical method. Ultimately, these results reveal that the semi-analytical method is helpful and provides an accurate analytical technique for evaluating PDE systems. In future, we will focus on applying this method to another model of a reaction–diffusion cell.

https://doi.org/10.1017/S1446181117000311 Published online by Cambridge University Press

## Acknowledgements

The author wishes to thank the anonymous referees for their useful comments.

## References

[1] M. Abramowitz and I. M. Stegun, *Handbook of mathematical functions* (Dover, New York, 1965).
[2] G. Adomian, *Solving frontier problem of physics: the decomposition method* (Kluwer Academic, New York, 1994).
[3] G. Adomian, "The diffusion-Brusselator equation", *Comput. Math. Appl.* **29** (1995) 1–3; doi:10.1016/0898-1221(94)00244-F.
[4] K. S. Al Noufaey and T. R. Marchant, "Semi-analytical solutions for the reversible Selkov model with feedback delay", *Appl. Math. Comput.* **232** (2014) 49–59; doi:10.1016/j.amc.2014.01.059.
[5] H. Y. Alfifi, T. R. Marchant and M. I. Nelson, "Generalised diffusive delay logistic equations: semi-analytical solutions", *Dyn. Contin. Discrete Impuls. Syst. Ser. B* **19** (2012) 579–596; http://online.watsci.org/contents2012/v19n4-5b.html.
[6] H. Y. Alfifi, T. R. Marchant and M. I. Nelson, "Semi-analytical solutions for the 1- and 2-D diffusive Nicholson's blowflies equation", *IMA J. Appl. Math.* **79** (2014) 175–199; doi:10.1093/imamat/hxs060.
[7] H. Y. Alfifi, T. R. Marchant and M. I. Nelson, "Non-smooth feedback control for Belousov–Zhabotinskii reaction–diffusion equations: semi-analytical solutions", *J. Math. Chem.* **57** (2016) 157–178; doi:10.1007/s10910-016-0641-8.
[8] M. R. Alharthi, T. R. Marchant and M. I. Nelson, "Mixed quadratic–cubic autocatalytic reaction–diffusion equations: semi-analytical solutions", *Appl. Math. Model.* **38** (2014) 5160–5173; doi:10.1016/j.apm.2014.04.027.
[9] W. T. Ang, "The two-dimensional reaction–diffusion Brusselator system: a dual-reciprocity boundary element solution", *Eng. Anal. Bound. Elem.* **27** (2003) 897–903; doi:10.1016/S0955-7997(03)00059-6.
[10] J. Biazar and Z. Ayati, "An approximation to the solution of the Brusselator system by Adomian decomposition method and comparing the results with Runge–Kutta method", *Int. J. Contemp. Math. Sci.* **2** (2007) 983–989; doi:10.1.1.558.4425.
[11] K. J. Brown and F. A. Davidson, "Global bifurcation in the Brusselator system", *Nonlinear Anal. Theory Methods Appl.* **24** (1995) 1713–1725; doi:10.1016/0362-546X(94)00218-7.
[12] T. Erneux, *Applied delay differential equations* (Springer, New York, 2009).
[13] C. A. Fletcher, *Computational Galerkin methods* (Springer, New York, 1984).
[14] G. Guo, J. Wu and X. Ren, "Hopf bifurcation in general Brusselator system with diffusion", *Appl. Math. Mech. (English Ed.)* **32** (2011) 1177–1186; doi:10.1007/s10483-011-1491-6.
[15] J. K. Hale, *Theory of functional differential equations* (Springer, New York, 1977).
[16] R. Jiwari and J. Yuan, "A computational modeling of two dimensional reaction–diffusion Brusselator system arising in chemical processes", *J. Math. Chem.* **52** (2014) 1535–1551; doi:10.1007/s10910-014-0333-1.
[17] S. Kumar, Y. Khan and A. Yildirim, "A mathematical modeling arising in the chemical systems and its approximate numerical solution", *Asia Pac. J. Chem. Eng.* **7** (2012) 835–840; doi:10.1002/apj.647.
[18] B. Li and M. X. Wang, "Diffusion-driven instability and Hopf bifurcation in Brusselator system", *Appl. Math. Mech. (English Ed.)* **29** (2008) 825–832; doi:10.1007/s10483-008-0614-y.
[19] B. Liu and T. R. Marchant, "The microwave heating of two-dimensional slabs with small Arrhenius absorptivity", *IMA J. Appl. Math.* **26** (1999) 137–166; doi:10.1093/imamat/62.2.137.
[20] M. Ma and J. Hu, "Bifurcation and stability analysis of steady states to a Brusselator model", *Appl. Math. Comput.* **236** (2014) 580–592; doi:10.1016/j.amc.2014.02.075.
[21] T. R. Marchant, "Cubic autocatalytic reaction diffusion equations: semi-analytical solutions", *Proc. R. Soc. Lond. A* **458** (2002) 873–888; doi:10.1098/rspa.2001.0899.

[22] T. R. Marchant and B. Liu, "The steady state microwave heating of slabs with small Arrhenius absorptivity", *J. Engrg. Math.* **33** (1998) 219–236; doi:10.1023/A:1004227904688.
[23] T. R. Marchant and M. I. Nelson, "Semi-analytical solution for one- and two-dimensional pellet problems", *Proc. R. Soc. Lond. A* **460** (2004) 2381–2394; doi:10.1098/rspa.2004.1286.
[24] R. C. Mittal and R. Jiwari, "Numerical study of two-dimensional reaction–diffusion Brusselator system", *Appl. Math. Comput.* **217** (2011) 5404–5415; doi:10.1080/15502287.2010.540300.
[25] R. Peng and M. X. Wang, "Pattern formation in the Brusselator system", *J. Math. Anal. Appl.* **309** (2005) 151–166; doi:10.1016/j.jmaa.2004.12.026.
[26] I. Prigogine and R. Lefever, "Symmetry breaking instabilities in dissipative systems. II", *J. Chem. Phys.* **48** (1968) 1665–1700; doi:10.1063/1.1668896.
[27] G. D. Smith, *Numerical solution of partial differential equations: finite difference methods* (Clarendon Press, Oxford, 1985).
[28] E. H. Twizell, A. B. Gumel and Q. Cao, "A second-order scheme for the Brusselator reaction–diffusion system", *J. Math. Chem.* **26** (1999) 297–316; doi:10.1023/A:1019158500612.
[29] J. G. Verwer, W. H. Hundsdorfer and B. P. Sommeijer, "Convergence properties of the Runge–Kutta–Chebyshev method", *Numer. Math.* **57** (1990) 157–178; doi:10.1007/BF01386405.
[30] A. M. Wazwaz, "The decomposition method applied to systems of partial differential equations and to the reaction–diffusion Brusselator model", *Appl. Math. Comput.* **110** (2000) 251–264; doi:10.1016/S0096-3003(99)00131-9.
[31] L. Xu, L. J. Zhao, Z. X. Chang, J. T. Feng and G. Zhang, "Turing instability and pattern formation in a semi-discrete Brusselator model", *Modern Phys. Lett. B* **27** (2013) 1–9; doi:10.1142/S0217984913500061.
[32] Y. You, "Global dynamics of the Brusselator equations", *Dyn. Partial Differ. Equ.* **4** (2007) 167–196; doi:10.4310/DPDE.2007.v4.n2.a4.